RAA 2020 Vol. **20** No. **10**, 166(14pp) doi: 10.1088/1674-4527/20/10/166

http://www.raa-journal.org *http://iopscience.iop.org/raa*

Research in Astronomy and Astrophysics

Some interesting topics provoked by the solar filament research in the past decade

Peng-Fei Chen (陈鹏飞)[1,2], Ao-Ao Xu (许敖敖)[3] and Ming-De Ding (丁明德)[1,2]

[1] School of Astronomy and Space Science, Nanjing University, Nanjing 210023, China; *chenpf@nju.edu.cn*
[2] Key Laboratory of Modern Astronomy & Astrophysics, Nanjing University, Nanjing 210023, China
[3] State Key Laboratory of Lunar and Planetary Sciences, Macau University of Science and Technology, Macau 999078, China

Received 2020 September 21; accepted 2020 October 5

Abstract Solar filaments are an intriguing phenomenon, like cool clouds suspended in the hot corona. Similar structures exist in the intergalactic medium as well. Despite being a long-studied topic, solar filaments have continually attracted intensive attention because of their link to coronal heating, coronal seismology, solar flares and coronal mass ejections (CMEs). In this review paper, by combing through the solar filament-related work done in the past decade, we discuss several controversial topics, such as the fine structures, dynamics, magnetic configurations and helicity of filaments. With high-resolution and high-sensitivity observations, combined with numerical simulations, it is expected that resolving these disputes will definitely lead to a huge leap in understanding the physics related to solar filaments, and even shed light on galactic filaments.

Key words: Magnetohydrodynamics — Sun: prominences — Sun: filaments

1 INTRODUCTION

As the closest star to humans, the Sun not only provides the necessary heat and light for life on Earth, but also exhibits a variety of intriguing activities, initially to the naked eyes and later through telescopes. Sunspots own the longest written record, which was made by Chinese in 165 BC (Wittmann & Xu 1987) or even 800 BC. Solar filaments might come off the second earliest, whose discovery was dated back to 1239 (Tandberg-Hanssen 1974).

Solar filaments are elongated dark features against the bright solar disk in various wavelengths such as Hα, Hβ, He I 10830 Å, Ca 8542 Å, Ca II H & K, Na D1, D2 & D3 as well as He I 304 Å. These are typical spectral lines formed at chromospheric temperatures, matching the thermal properties in filaments. Solar filaments are also identifiable as dark features in extreme ultraviolet (EUV) images, which is mainly attributed to volume blocking (Heinzel et al. 2003). When solar filaments move to the solar limb following solar rotation, they are revealed to be suspended above the solar limb. In this case, they are called prominences. Solar filaments and prominences are generally used interchangeably in the literature.

Talking about solar prominences, we have to mention that historically any plasma structure standing out of the solar limb was called a prominence (de Jager 1959; Zirin 1988), including surges, spicules and postflare loops. In the modern semantic environments, these dynamic phenomena are not classified as prominences. Another similar phenomenon is the so-called arch filament systems (Su et al. 2018), which look very similar to solar filaments in Hα images, consisting of many threads. However, arch filament systems are short-lived dynamic structures associated with emerging magnetic flux. As a result, they are very different from solar filaments in Dopplergrams: Their central part displays blueshifts and the footpoints of their threads display redshifts. Moreover, one key difference between solar filaments and arch filament systems is that the threads in the former are generally weakly skewed from the magnetic neutral line, whereas the threads in arch filament systems are quasi-perpendicular to the underlying magnetic neutral line.

Another issue worth clarifying is whether solar filaments should be called a chromospheric structure or a coronal structure, both of which were used in the literature. The temperature of filament plasma is in the range of 6000–8000 K, which is the typical temperature of the solar chromosphere. This is why solar filaments are most discernable in the Hα line, which is widely employed to observe the chromosphere. However, we are strongly against the statement describing solar filaments

as chromospheric structures. We stress here that solar filaments are cold structures suspended in the hot corona and thus are coronal structures. A filament might be rooted at the solar chromosphere, or it might also hang totally well above the solar chromosphere.

Filaments are a fascinating phenomenon in the solar atmosphere not only for their stunning appearance, but also for the physics involved in the whole lifelong evolution: (1) Their formation is related to thermal instability, which is fighting all the time with coronal heating. We tend to believe that the secret about how the corona is heated is partly hidden in the process of how the coronal plasma cools down to form filaments. In particular, the thermal discontinuities brought by filaments provide a favorite environment for magnetic energy deposit (Low 2015). (2) Their oscillations and dynamics can be utilized to diagnose the coronal magnetic field that cannot be measured precisely to date (Arregui et al. 2018). (3) Their eruptions are intimately related to solar flares and coronal mass ejections (CMEs, Chen 2011), the two major eruptions in the solar atmosphere that might pose disastrous disturbances to the space environment near the Earth. This is why it was stated that solar filaments, once erupting, are not only the core of CMEs, but also the core of CME research (Chen et al. 2014). From a longer timescale point of view, solar filaments trace the magnetic neutral lines associated with active regions and decayed active regions, their latitude evolution displays a butterfly diagram similar to sunspots (Hao et al. 2015), and they display the same hemispheric asymmetry as sunspots (Li et al. 2010a; Kong et al. 2015). Because of the importance of solar filaments, many monographs and review papers were devoted to this topic (Parenti 2014; Vial & Engvold 2015; Gibson 2018). In this review, rather than covering every aspect of filament research, we will focus mainly on some new or controversial topics that were provoked in the past decade and are in strong need of clarification.

This paper is organized as follows. After compiling what we have known about solar filaments in Section 2, we discuss in detail those debated issues or newly proposed ideas in solar filament research in Section 3, and some less touched upon but worthwhile topics are mentioned in Section 4.

2 WHAT WE HAVE ALREADY KNOWN

2.1 Filament Formation

While the cosmic background radiation cools down monotonically after the big bang, the baryonic matter in the universe struggles between superhot (10^6–10^7 K) states and supercold (10–10^3 K) owing to the competitive interplay between various kinds of heating and runaway radiative cooling, making mixing structures with different sizes. On large scales like tens of kpc, one example of the mixture of cold and hot plasmas is the cold galactic filaments embedded in the hot galactic corona. On smaller scales like tens of Mm, a typical example is solar filaments, which correspond to $\sim$7000 K plasma embedded in the 10^6 K solar corona.

Early in 1950s, Parker (1953) proposed that cold filaments are formed due to thermal instability where thermal conduction is the restoring process. Two factors contribute to such thermal instability. First, the radiative cooling rate is proportional to n_e^2, whereas the coronal heating rate is proportional to n_e or insensitive to n_e depending on the heating mechanisms, where n_e is the electron density in the corona. Therefore, a perturbation with a negative ΔT and positive Δn (keeping the gas pressure unchanged) would lead to further cooling. Second, the radiative loss function increases with the decreasing temperature T in the range of $T > 2 \times 10^5$ K. It means that a perturbation with a negative ΔT in the 10^6 K corona enhances radiative cooling, and a runaway instability happens.

For two reasons it is believed that the filament material does not come from the quiet corona itself. First, the element abundance of many filaments is similar to that of the low solar atmosphere and different from that of the corona (Spicer et al. 1998; Song et al. 2017). This means that the plasma in the photosphere and chromosphere should somehow fill in the filaments that are high up in the corona. Second, the plasma density inside the filament is $\sim$100 times higher than that of the ambient corona, and the typical length of a filament thread is $\sim$10 Mm (Lin et al. 2005). This means that the magnetic flux tube should be larger than 10^3 Mm, which is almost 10 times the typical magnetic field length in filament channels. It implies that there is no sufficient mass in the coronal portion of the in situ magnetic flux tubes to feed a long filament thread. It is noted in passing that it was often claimed that the mass of 10 quiescent filaments is roughly the total mass of the entire corona (Malherbe 1989), which might not be precise. The typical mass of a filament is $\sim 10^{14}$–2×10^{15} g (Parenti 2014), whereas the mass of the corona from the bottom to an altitude of 0.2 $R_\odot$ amounts to $\sim 6 \times 10^{17}$ g.

The straightforward solution is that the chromospheric cool plasma is heated locally to evaporate into the corona, where the hot and dense plasma cools down owing to thermal instability. Such a mechanism is sometimes called the chromospheric evaporation–coronal condensation model or evaporation–condensation model for short (Antiochos et al. 2000). It was further found that if the ratio of apex to footpoint heating rates is less than $\sim$0.1 and asymmetries in heating and/or cross-sectional area are less than $\sim$3, no equilibrium can be reached in the whole magnetic loop, which is called thermal non-equilibrium. The corona either keeps evolving in a limit cycle with

changing temperatures or condenses into a filament near magnetic dips (Klimchuk 2019). In the latter case, it should be the thermal instability that leads the coronal plasma to a lower temperature rather than a higher temperature. The condensation process was verified by observations from the Atmospheric Imaging Assembly (AIA) aboard the Solar Dynamics Observatory (SDO, Berger et al. 2012; Liu et al. 2012b). Besides chromospheric evaporation, which triggers thermal instability via enhancing plasma density, it is interesting to note that adiabatic expansion of the coronal loops might do the same job by decreasing the temperature of the coronal loop (Lee et al. 1995).

The second mechanism of filament formation is the direct injection of chromospheric plasma into the corona (Wang 1999; Wang et al. 2018b, 2019b). Different from the evaporation–condensation model or the thermal non-equilibrium model, where filaments appear in the corona from nothing in Hα observations, the injection mechanism is manifested as direct injection of Hα surges across the filament channel. In this scenario, the filament threads might be quasi-perpendicular to the underlying magnetic neutral line, rather than quasi-parallel with the magnetic neutral line, as seen from Figure 7 of Zou et al. (2016).

The third formation mechanism is the so-called levitation model, where chromopheric plasma is lifted along with emerging flux (Rust & Kumar 1994), which was occasionally observed (Xu et al. 2012). Magnetohydrodynamic (MHD) simulations indicated that chromospheric magnetic reconnection might facilitate the levitation of heavy filaments (Zhao et al. 2017). If the emerging flux is a flux rope, we expect to see an arch filament system (which corresponds to the top part of the flux rope), followed by a filament. The threads in the arch filament system and the filament should be oppositely skewed from the magnetic neutral line.

It should be kept in mind that the Sun is always more complicated than we think. Filaments might be formed in a way quite different from the above-mentioned models. For example, it was recently proposed that magnetic reconnection in the low corona can also trigger thermal instability, leading to filament formation (Kaneko & Yokoyama 2017). Such a process was confirmed by SDO/AIA observations (Li et al. 2019d). In this case, the mass source is the corona itself, and no chromospheric evaporation is needed (unless reconnection-accelerated electrons bombard the chromosphere to generate chromospheric evaporation). It is expected that the element abundance in this type of filament should be the same as that of the corona. Moreover, it is noticed that there are ubiquitous chromospheric fibrils, among which the fibrils near sunspots are longer than those in quiet regions (Jing et al. 2019). Filaments can also be formed due to the interactions between neighboring fibrils or between a fibril and a superpenumbral filament, where magnetic reconnection was proposed to be the key (Bi et al. 2012; Xue et al. 2016; Yan et al. 2016; Yang et al. 2016a,b).

2.2 Filament Oscillations

Any object in equilibrium is subject to external perturbations, and may inevitably deviate from the equilibrium position. If the restoring force is strong enough, the object can come back, leading to oscillations. With various types of energy dissipation mechanisms such as viscosity and radiation, the kinetic energy, which can be as large as 10^{26} erg (Shen et al. 2014a), would finally damp out. Therefore, oscillations can provide vital information on the triggering process, restoring force and damping mechanisms. Moreover, filament oscillations without significant decay might be a precursor for filament eruptions and CMEs (Chen et al. 2008; Li & Zhang 2012; Zheng et al. 2017). As a result, there has been booming research on filament/prominence oscillations, and prominence seismology has been progressing rapidly (Arregui et al. 2018).

Based on the nature of the restoring force, filament oscillations can be divided into longitudinal oscillations and transverse oscillations. In the former case, the filament plasmas oscillate along the magnetic field lines, hence the Lorentz force $\mathbf{J} \times \mathbf{B}$ does not affect the motion, and the restoring force includes the field-aligned component of gravity and the gas pressure difference between the two ends of the filament thread (Luna & Karpen 2012; Zhang et al. 2012). It was found that the gravity component is the dominant one unless the magnetic dip is too shallow. In the case of transverse oscillations, the plasma and frozen-in magnetic field move perpendicularly to the magnetic field, where Lorentz force takes effect (Shen et al. 2014b; Zhou et al. 2018). As a result, the period of longitudinal oscillations is generally of the order of 1 hr, whereas that of transverse oscillations is around $\sim$20 min. Caution is warranted in that the period for each mode has a wide range.

It is not as straightforward as we thought to identify the oscillation mode (Pant et al. 2015, 2016; Chen et al. 2017b). Whether it is longitudinal or transverse depends on whether the plasma motion is along or perpendicular to the magnetic field. There was misunderstanding in the literature claiming that longitudinal oscillations are along the filament axis or attributing any lateral displacement to transverse oscillations. Noticing that the magnetic field lines follow the threads, which deviate from the filament axis (or spine) by 10°–30° (Hanaoka & Sakurai 2017), even longitudinal oscillations would present displacement perpendicular to the filament spine.

Depending on the attack angle relative to the filament threads, a large-scale coronal shock wave might cause longitudinal oscillations in one filament and transverse

oscillations in the other (Shen et al. 2014b), or even no response from a low-lying filament (Liu et al. 2013). The co-existence of longitudinal and transverse oscillations in one filament recently attracted much attention (Pant et al. 2016; Wang et al. 2016a; Zhang et al. 2017a; Mazumder et al. 2020). Whether the two modes are excited separately or there is mode conversion is definitely another interesting topic (Liakh et al. 2020).

Once an oscillation mode is determined, its period can be used to diagnose the magnetic field strength and configuration in the corona. For example, in terms of longitudinal oscillations, the period was applied to derive the curvature radius of the local magnetic dip (Luna & Karpen 2012; Zhang et al. 2012; Zhou et al. 2018). The curvature evolution can also be deciphered, e.g., when a filament is activated to rise slowly, its longitudinal oscillation period was observed to increase, implying that the magnetic dip became flatter and the flux rope became less twisted (Bi et al. 2014). It was also observed that the oscillation period increases in some threads but decreases in other threads of the same filament, implying correlated magnetic rearrangement (Zhang et al. 2017b). In terms of transverse oscillations, the period was utilized to estimate the magnetic field strength around the filaments (Zhou et al. 2018). For example, Zhang & Ji (2018) applied the seismology to an oscillating prominence and found that the magnetic field in the cavity is less than 10 G.

As an important ingredient of prominence seismology, the decay time of filament oscillations also discloses vital information. For longitudinal oscillations, the simulation results of Zhang et al. (2012, 2020a) indicated that radiative cooling and thermal conduction are not sufficient to explain the decay, and extra factors should be taken into account. Extra damping mechanisms include mass drainage (Zhang et al. 2013), mass accretion (Ruderman & Luna 2016), wave leakage (Zhang et al. 2019) and increase of the background coronal temperature (Ruderman & Luna 2016). The longitudinal oscillations can be amplified by additional perturbations (Zhang et al. 2020a) or the decrease of the background coronal temperature (Ruderman & Luna 2016). For transverse oscillations, Adrover-González & Terradas (2020) proposed that resonance absorption is the main mechanism. Wave leakage might play a role as well.

2.3 Filament Eruptions

Filaments end their lives by either thermal disappearance or eruptions. Their thermal disappearance might be due to enhanced coronal heating or mass drainage without further mass replenishment. Their eruptions can be successful or failed ones. For successful eruptions, the whole picture can be explained by the standard flare/CME model, where magnetic reconnection plays a crucial role (Chen 2011). Although the model holds true in principle, it is basically a schematic sketch, with many details waiting to be supplemented. In the past decade, most advances were concentrated on the new characteristics brought by 3-dimensional (3D) magnetic reconnection compared to its 2-dimensional (2D) counterpart (Mei et al. 2017) and some new features brought by the complex background magnetic field. For example, non-uniform or reconnection-favored background magnetic field (including multiple spine-fan configurations) might lead to rich dynamics of the ejecta that cannot be accounted for in the original standard model, such as deflection, splitting, disintegration, mass transfer and even rotation (Bi et al. 2013; Wang et al. 2016b; Yang et al. 2015b; Li et al. 2016; Chen et al. 2018a; Liu et al. 2018a; Li et al. 2019b; Wei et al. 2020; Yan et al. 2020). A hot channel is also formed due to magnetic reconnection, which maps the flux rope with the erupting cool filament at the bottom (Cheng et al. 2014a). We tend to link this hot channel to the fuzzy component observed in the CME core (Song et al. 2019a).

More attention was paid to the triggering mechanisms (Zhang et al. 2020b), which can be divided into ideal MHD type and reconnection type. Sometimes, the two types of processes might work together (Song et al. 2015). In the past decade, plenty of efforts were made on ideal MHD mechanisms (Bi et al. 2015; Mei et al. 2018), such as kink instability and torus instability. Contradictory results were obtained on whether the threshold of the torus instability is similar (Xing et al. 2018) or different (Zou et al. 2019b) between active-region filaments and quiescent filaments. One uncertain issue in these works is whether slow magnetic reconnection is already going on during the claimed ideal MHD triggering process. A possible signature of such slow reconnection is the appearance of the EUV hot channel before the impulsive phase of the associated flare in many events. Noticing that torus instability was sometimes considered to be the driving mechanism for the full eruption rather than a triggering mechanism (see Schmieder et al. 2015, for a review), Chen (2019) doubted this by a logic test: Suppose the decay index of the background magnetic field exceeds the threshold of the torus instability everywhere from the low corona all the way to interplanetary space, then can a 3D flux rope erupt to form a CME purely due to torus instability? If it could, this process would violate the Aly-Sturrock constraint.

Several possible reasons for erupting filaments to fail were explored. They can be hindered by overlying arcades (Chen et al. 2013), gravity (Filippov 2020), filament rotation (Zhou et al. 2019), or another filament lying above (Jiang et al. 2014b). There are also events where a part of the filament erupts successfully and the other part fails (Zhang et al. 2015).

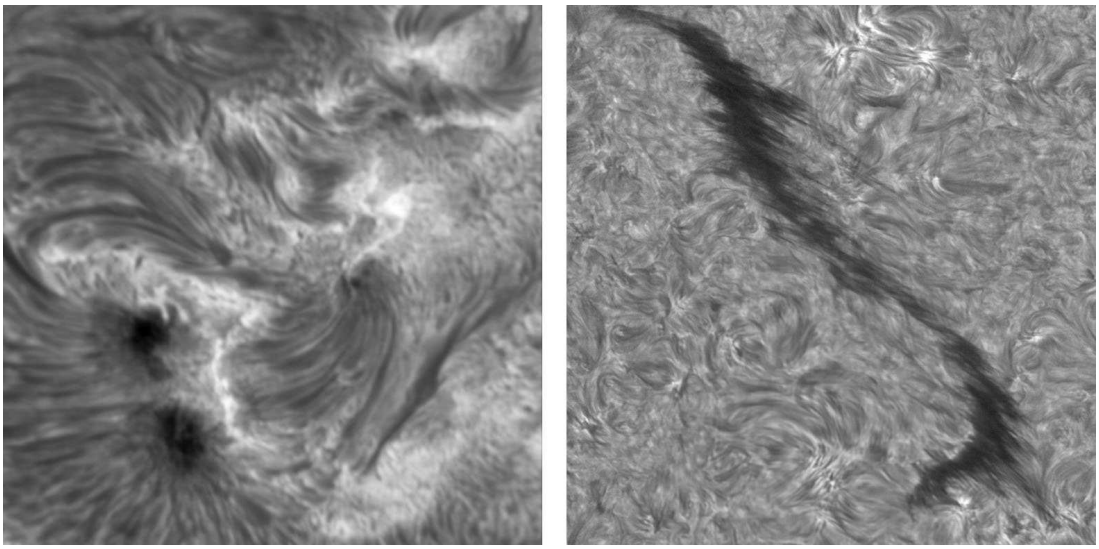

Fig. 1 Solar filaments observed by the New Vacuum Solar Telescope in Hα. *Left panel*: several active region filaments around two sunspots; *Right panel*: a quiescent filament.

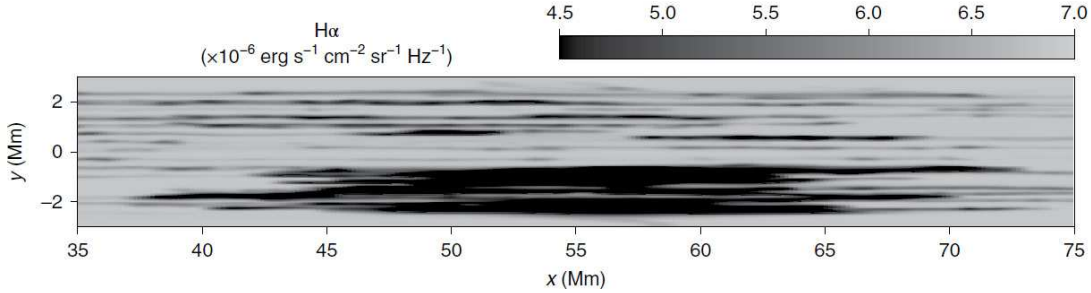

Fig. 2 Synthesized Hα image of a filament in MHD simulations, showing a filament is composed of many thin threads. Taken from Zhou et al. (2020a).

3 SOME NEW OR CONTROVERSIAL TOPICS

3.1 Fine Structures

Figure 1 displays several active region filaments (left panel) and a quiescent filament (right panel), both of which were observed by the Chinese New Vacuum Solar Telescope (NVST, Liu et al. 2014). Fine structures can be seen clearly. It is generally claimed that a filament is composed of a spine and a few barbs. We have to stress here that the spine is not a real structure, at least not for a quiescent filament. As indicated by the right panel of Figure 1, filament threads are actually the building blocks of a filament. The illusion of a spine is simply due to the fact that all the threads are situated above the magnetic neutral line. Our statement may hold true even for active-region filaments, though their threads are nearly parallel with the magnetic neutral line.

Although it is well known that threads are the building blocks of filaments (Lin et al. 2005), one question that has not been asked is why filaments exist in the form of a collection of threads, rather than being clumpy. To answer this question, Zhou et al. (2020a) performed 2D MHD simulations with a high spatial resolution, by which they proposed that turbulent heating in the solar surface drives random chromospheric evaporation, leading to sporadic coronal condensation in some magnetic dips. Once a thread is born, its gas pressure decreases as demonstrated by Xia et al. (2011), which results in the shrinkage of the local flux tube and the expansion of the neighboring flux tubes (hence low density). It implies that once a thread is formed, its neighboring flux tubes become unfavored space for coronal condensation. They also found that the filling factor of threads in a filament channel is proportional to the strength of the chromospheric heating, which can explain why some filaments look seamless, in particular those filaments in active regions, where the heating is much stronger than in quiet regions. As depicted in Figure 2, the threads have a length from several to 30 Mm, and an average width of 100 km. They occupy 10%–15% of the space in the filament channel. All these are consistent with observations (Lin et al. 2005).

Prominences, especially quiescent prominences, show more complicated fine structures, with many vertical

threads as well as dark plumes emerging from the low-lying bubbles, as seen in Figure 3 (Berger et al. 2011; Li et al. 2018a). It is still unclear how these vertical threads are formed. Are their magnetic field lines oriented vertically or mainly horizontal but turbulent? Xia & Keppens (2016b) performed 3D MHD simulations, and proposed that magnetic Rayleigh-Taylor instability turns an initially horizontal magnetic field into turbulent, forming vertical threads. A parade of vertical threads forms apparently horizontal threads. In this model, the horizontal threads are apparent structures. Schmieder et al. (2014) and Ruan et al. (2018) held a different viewpoint, claiming that the magnetic field is mainly horizontal, and the vertical threads in quiescent prominences are apparent structures due to piling up of a series of small dips. With coronal magnetic extrapolations, Su et al. (2015) found that the vertical threads in a polar crown prominence are supported by horizontal dips in a flux rope, implying that the field lines crossing the prominence are horizontal. There is a similar debate on whether the filament threads on the solar disk are field-aligned (Zhou et al. 2020a) or field-misaligned (Claes et al. 2020).

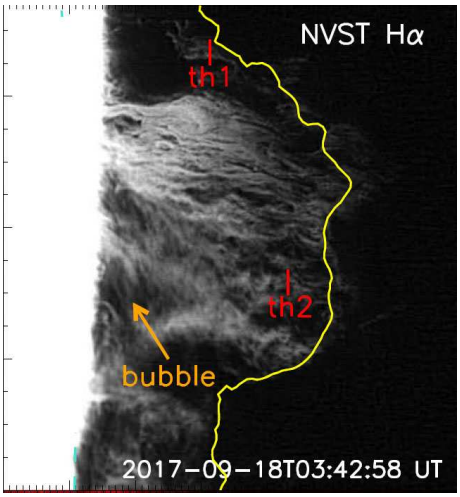

Fig. 3 A prominence above the solar limb observed by NVST in Hα, featuring vertical threads, plumes and bubbles. Taken from Li et al. (2018a).

3.2 Chirality and Helicity

Similar to many other natural phenomena like typhoons on the Earth, solar filaments also possess chirality. From the magnetic perspective, imagine that we stand on the positive polarity side of a filament channel; if the axial magnetic field in the filament is toward left, the filament is called sinistral; if the axial magnetic field in the filament is toward right, the filament is called dextral (Martin et al. 1992). The corresponding current helicity $H_c = \mathbf{J} \cdot \mathbf{B}$ is positive/negative in sinistral/dextral filaments. From the Hα or EUV image perspective, filament barbs are either left-bearing (like the highway exits in Japan) or right-bearing (like the highway exits in China). Martin (1998) proposed a correlation between these two types of chirality, i.e., left-bearing/right-bearing barbs correspond to sinistral/dextral filaments. In other words, filaments with left-bearing/right-bearing barbs have positive/negative helicity. This correspondence provides a handy approach to identify the sign of helicity simply from Hα or EUV images. As a result, this approach has been widely applied to investigate the hemispheric rule of helicity.

However, Guo et al. (2010) found both left- and right-bearing barbs in one filament with negative helicity. Their coronal magnetic extrapolation indicated that the filament segment with the left-bearing barb is supported by a sheared arcade, whereas the filament segment with the right-bearing barb is supported by a flux rope. Along this line of thought, Chen et al. (2014) put forward that Martin's rule is correct only for the filaments supported by flux ropes, and the correspondence between the barb bearing and the helicity sign is opposite for the filaments supported by sheared arcades. They noticed that once a filament erupts, some materials drain down to the solar surface, producing twin brightenings on the two sides of the magnetic neutral line. The twin drainage sites also exhibit chirality, i.e., they are either left skewed or right skewed relative to the magnetic neutral line. Chen et al. (2014) proposed that left-skewed twin drainage sites correspond to negative helicity and right-skewed drainage sites correspond to positive helicity. A similar scheme was already proposed by Wang et al. (2009), though with a distinct explanation. Applying this approach to 571 erupting filaments observed by SDO/AIA during May 2010–December 2015, Ouyang et al. (2017) ascertained that 91.6% of these filaments follow the hemispheric rule of helicity sign, i.e., negative/positive in the northern/southern hemisphere. They also investigated the cyclic evolution of such a hemispheric rule, and found that the hemispheric preference of quiescent and intermediate filaments stays significant in the whole solar cycle, but that of active-region filaments can disappear near solar maximum or minimum. The coronal helicity is contributed by both magnetic flux emergence and surface motions. The significant hemispheric preference of the quiescent and intermediate filaments tends to support the helicity condensation model (Antiochos 2013; Knizhnik et al. 2017), where helicity injected from the solar surface due to small-scale rotational flows inversely cascades from small scales to large scales. The rotational flows are supposed to be driven by the Coriolis force acting on the granular or supergranular flows.

3.3 Magnetic Configuration

The magnetic configuration of solar filaments is an extremely important research topic since filaments are the source regions of many flare/CME events. Before going into the details, we first comment on the question of whether it is necessary for a filament to be supported by magnetic dips, which were originally proposed to balance the gravity last century. With numerical simulations, Karpen et al. (2001) demonstrated that even in a simple magnetic loop without any dips, chromospheric evaporation–coronal condensation can also happen, leading to repeated thread forming and draining. In addition, for the filaments arising from the injection mechanism (Wang 1999), cold chromospheric material is injected into the coronal loop from one end and drains down to the other end of the magnetic field line. Hence, magnetic dips are not necessary either. Unfortunately, the coronal magnetic field is still an important parameter that we cannot measure directly with sufficiently high precision. However, one important clue from observations is that if we can observe longitudinal oscillations (including the small-amplitude counterstreamings) in the filament threads, we can judge that magnetic dips exist in these filaments. We are reminded that we cannot simply exclude magnetic dips when longitudinal oscillations are not observed. Although no survey has been taken to determine the percentage of the filaments with magnetic dips, our impression based on the above clue is that a large number of filaments are supported by magnetic dips. Therefore, we focus on these filaments in the rest of this subsection.

Suppose there is a filament channel with positive magnetic polarity on the left side and negative polarity on the right side, then there are two types of magnetic dips above the magnetic neutral line in the corona: normal-polarity dips with magnetic field pointing to the right and inverse-polarity dips with magnetic field pointing to the left. The typical corresponding magnetic configurations are a sheared arcade and a flux rope, which are displayed in Figure 4. As mentioned in Gibson (2018, and references therein), there is also a normal-polarity flux rope model. However, this model was sketched in 2D. When mapped to 3D space where the flux rope is rooted to the solar surface, a problem of mixed chirality arises.

There were sporadic measurements of magnetic fields inside prominences, which are not routinely available nowadays. However, Chen et al. (2014) proposed an indirect way to distinguish these two types of magnetic configurations based on EUV or Hα images only: If the helicity of a filament channel is positive/negative and the filament barbs or threads are left/right bearing, then the filament is supported by a flux rope; If the helicity of a filament channel is positive/negative and the filament barbs or threads are right/left bearing, then the filament is supported by a sheared arcade. This method is illustrated in Figure 5, according to which the famous scheme proposed by Martin (1998) holds true only for the filaments supported by flux ropes. Applying this method to 571 filaments observed by SDO/AIA, Ouyang et al. (2015, 2017) found that 89% of the filaments are supported by flux ropes and 11% are by sheared arcades. Such a ratio is similar to that obtained from coronal magnetic extrapolations (Duan et al. 2019).

The widely used method to decipher the filament magnetic configuration is still the magnetic extrapolation based on photospheric vector magnetograms (Su et al. 2015; Guo et al. 2017, 2019; Mackay et al. 2020; Zhu et al. 2020). Whereas sheared arcades were paid less attention, most papers were devoted to the events with flux ropes (see Cheng et al. 2017; Liu 2020, for reviews). For these papers, while many extrapolations showed that the flux ropes before eruption are generally weakly twisted (Jiang et al. 2014a; Li et al. 2017), several authors claimed that highly twisted flux ropes can nicely match the filament geometry or spectro-polarimetric observations (Guo et al. 2019; Mackay et al. 2020). The corresponding twist is larger than three turns, which is well above the threshold of kink instability (Hood & Priest 1981). If highly-twisted flux ropes can be stable, one possible reason might be that the gravity hinders the filaments from erupting (Fan 2020), which significantly increases the threshold of kink instability. Highly-twisted flux ropes imply that there are multiple dips, hence multiple threads, along one flux tube, which brings new topics. For example, the thread longitudinal oscillations are no longer independent, and there is thread-thread interaction, which significantly changes the damping time of the oscillations, sometimes leading to decayless oscillations (Zhou et al. 2017). The signatures of such thread-thread interaction were found in observations (Zhang et al. 2017b).

With high-resolution and high-sensitivity observations, the magnetic configurations of some filaments can be mapped by tracing the plasma motions when filaments are activated. In this way, the twist of the coronal magnetic field can be estimated, which was found to range from 1π to 6π in different events (Yan et al. 2014; Yang et al. 2014; Hou et al. 2016; Chen et al. 2019; Shen et al. 2019; Xu et al. 2020). The lower limit might correspond to a sheared arcade, while others to a flux rope.

It is noted that not all magnetic configurations can be exclusively classified as a sheared arcade or a flux rope. A filament might be supported by a flux rope in a segment and by a sheared arcade in the other (Guo et al. 2010). Besides, the existence of double-decker filaments requires a combination of the two elementary configurations, i.e., sheared arcade plus sheared arcade, flux rope plus flux rope and sheared arcade plus flux rope. The method proposed by Chen et al. (2014), see Figure 5, can be

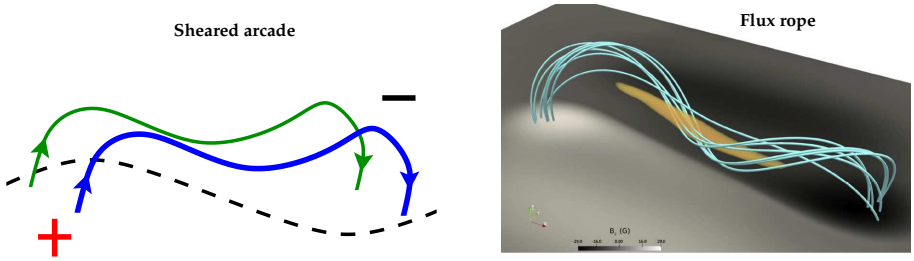

Fig. 4 Two types of magnetic configurations for solar filaments. *Left panel*: A sheared arcade with normal polarity dips; *Right panel*: A flux rope with inverse-polarity dips. The right panel is taken from Zhou et al. (2018).

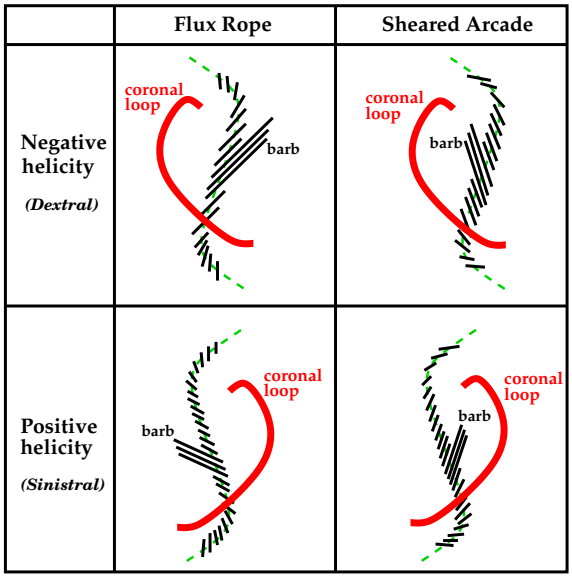

Fig. 5 Schematic sketch demonstrating the correspondence between the helicity and the chirality of the filament barbs (*longer black lines*), threads (*shorter black lines*) and the overlying coronal loops (*red lines*) in two magnetic configurations, i.e., flux ropes and sheared arcades. The green dashed lines mark the magnetic neutral lines of filament channels.

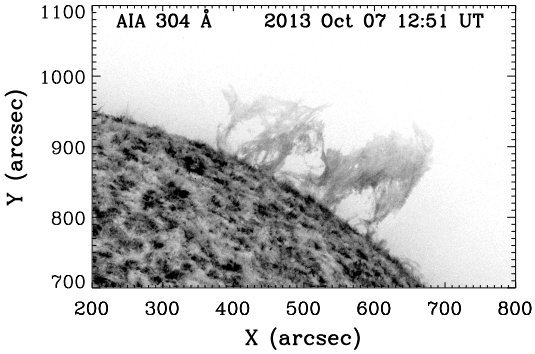

Fig. 6 A solar prominence observed by SDO/AIA at 304 Å on 2013 October 7, featuring several feet attached to the solar surface. This figure is a negative image.

employed to discriminate these possibilities. The double-decker filaments may erupt in different ways depending on the background magnetic field (Kliem et al. 2014): Maybe the upper branch erupts, leaving the lower branch almost intact (Cheng et al. 2014b; Zheng et al. 2019), or the lower branch erupts first, which then pushes the upper branch to erupt after coalescence (Zhu et al. 2015). Interestingly, there are events with magnetic configurations similar to the double-decker filaments, but no cool material exists in the upper branch of the magnetic structure. In this case, as the upper branch erupts, an erupting hot channel is visible, but the lower filament remains intact (Liu et al. 2018b).

3.4 How Filament Barbs Are Formed

As indicated by Figure 1, filament barbs are indeed an eminent ingredient of a filament, which veer away from the apparent spine. Generally, active region filaments have less barbs (some even have no barbs), whereas quiescent filaments have more barbs. According to the statistical research of Hao et al. (2015), about 75% of filaments have less than five barbs, and a small portion of filaments have more than ten barbs. Li & Zhang (2013) studied a polar crown filament which had 69 barbs. According to their results, the formation of filament barbs is associated with three types of plasma motions, and the disappearance of barbs is also accompanied by three types of plasma motions that are influenced by the changing photospheric magnetic field.

When a filament lies above the solar limb as a prominence, it often has several feet, as displayed in Figure 6. It is generally taken for granted that a filament barb corresponds to the projection of a lateral foot, which extends down to the solar surface. With a linear force-free magnetic field extrapolation, Aulanier & Demoulin (1998) proposed that the intrusion of a parasitic polarity into a bipolar filament channel would produce a series of new magnetic dips, which extends from the main flux rope to the solar surface. If these new magnetic dips are filled with cold plasma, they match the observed filament barbs very well when seen from above. Such a lateral dip assembly model can explain many filament barbs (Chae et al. 2005).

Interestingly, recent observations indicated that there might exist another type of barbs, which are due to

longitudinal oscillations of some threads in the filament, and hence are called "dynamic barbs" (Awasthi et al. 2019). With quadrature observations from SDO and STEREO-B, Ouyang et al. (2020) confirmed that the dynamic barbs are due to longitudinal oscillations, and the barb does not extend down to the solar surface. Hence, they proposed that a filament barb does not always correspond to a prominence foot. Similarly, when some threads drain down along the field line, a transient barb is also visible (Xia et al. 2014).

In addition, if the magnetic dips are not identical, with some dips much longer than others, their threads would be much longer than other threads as well since the length of a thread is proportional to the length of the magnetic dip (Zhou et al. 2014). In this case, a barb would also be present without the help of parasitic magnetic polarity in the filament channel. Since this type of barb is simply due to local longer threads, it is expected that such filament barbs do not correspond to prominence feet as well.

3.5 The Nature of Counterstreamings

Similar to the quiet Sun, which is never really quiet, any filament is never static even when the whole appearance looks invariant with time. Flows and small-scale oscillations are ubiquitous. It is estimated that filament material drains down to the solar surface at a rate of $\sim 10^{15}\,\mathrm{g\,day^{-1}}$ (Liu et al. 2012b), implying that the plasma of a filament is recycled completely on the timescale of $\sim$1 day. MHD simulations verified such mass cycling (Xia & Keppens 2016a).

Spectroscopic observations indicated that redshifted and blueshifted motions are pervasive in the filament threads (Schmieder et al. 1991), which were later called counterstreaming flows (Zirker et al. 1998). The classical model attributed them to filament thread longitudinal oscillations (Lin et al. 2005). Indeed, different magnetic dips have different curvature radii, leading to different oscillation periods according to the pendulum model. Moreover, perturbations imposed on individual threads are often random. These two factors result in the longitudinal oscillations being out of phase, i.e., some are forward and some are backward, forming counterstreamings.

On the other hand, Chen et al. (2014) proposed that the counterstreaming flows have another component, i.e., unidirectional flows with opposite directions. This scenario was confirmed by various observations (Yan et al. 2015; Li & Zhang 2016; Zou et al. 2016; Wang et al. 2018a). Therefore, it is expected that some counterstreamings are due to filament thread longitudinal oscillations, some are due to unidirectional flows, and some are due to their combination as demonstrated in numerical simulations (Zhou et al. 2020a) and observations (Diercke et al. 2018; Wang et al. 2018a; Panesar et al. 2020). It is also conceivable that for the filaments formed via the injection mechanism (Wang 1999), their counterstreamings tend to be mainly due to unidirectional flows. Furthermore, Zhou et al. (2020a) proposed that hot counterstreaming flows exist in the interthread corona, which are purely due to unidirectional flows.

The counterstreamings mentioned above are horizontal flows along magnetic field lines, therefore they are mostly observed in filaments on the solar disk as proper motions or in prominences above the solar limb as Doppler-shifted patterns. With high-resolution observations, vertical threads in the hedgerow prominences also present complicated upward and downward motions (Berger et al. 2011), which were called vertical counterstreamings by Shen et al. (2015). This type of upward and downward flows is also visible in filament barbs, and their formation was suggested to be a mixture of simultaneous flows, waves and magnetic field motions (Li & Zhang 2013; Kucera et al. 2018). This is definitely a topic deserving further research.

3.6 The Nature of Solar Tornados

Generally speaking, filaments on the solar disk exhibit much simpler morphology compared to prominences above the solar limb, even when the spatial resolution of the observations is not high. Such an overlooked characteristic might actually have a profound implication: threads, the building blocks of filaments, are generally situated on horizontal magnetic flux tubes. Therefore, when viewed from above, we can see the whole thread, and all the quasi-parallel threads lining up along the magnetic neutral line show simple morphologies. When viewed from the side as in the case of prominences, the thread assembly might make up any pattern due to projection effects, especially when the threads are roughly along the line of sight. As a result, even in the 1930s, Pettit (1932) classified solar prominences into five classes, one of which is tornado-like.

With their high-resolution, SDO/AIA observations revealed many tornado-like structures not only at the bottom of a coronal cavity (Li et al. 2012) but also in filament feet/barbs (Su et al. 2012). Li et al. (2012) interpreted the vortex-like motions as a combination of mass flows and density waves propagating along the helical magnetic fields, whereas Su et al. (2012) interpreted the tornado feet of the filaments as rotating magnetic structures driven by the underlying vortex flows on the solar surface. Su et al. (2012) argued that solar tornados play an important role in supplying mass and magnetic twists into the filaments. In this explanation, the filament feet are similar to rotating macrospicules, which were also called solar tornados (Pike & Mason 1998). Later, Su et al. (2014) investigated the dynamics of the

immediately ambient coronal plasma around a tornado with the Hinode/EIS spectral data. With opposite velocities of $\sim$5 km s^{-1} persisting for more than 3 h on the two sides of the tornado, they concluded that the blue- and red-shifted motions across the tornado are consistent with their rotation model. One query this model is confronted with is whether the persistent twisting motion would transfer too much twist into the filament body so that the filament becomes kink unstable.

Several authors proposed alternative explanations. Panasenco et al. (2014) suggested that the apparent rotation motions in the solar tornados are an illusion due to counterstreamings of the threads inside the filament feet. In this case, each thread in the filament foot experiences longitudinal oscillations around the local magnetic dip, and all the longitudinal oscillations out of phase would give an illusion that the filament foot is rotating. Spectroscopic observations can definitely provide additional information in discriminating apparent motions from mass motions, and hence can shed light on the nature of the solar tornados. Schmieder et al. (2017) observed a tornado with the MSDP spectrograph, and the derived Hα Doppler maps feature a pattern with alternatively blueshifted and redshifted areas 5″-10″ wide. More importantly, the blue- and red-shifts change sign with a quasi-periodicity of 40–60 min, supporting the idea that the threads inside the tornado are oscillating along the basically horizontal magnetic dips, which are mainly oriented along the line of sight. The longitudinal oscillations out of phase in different magnetic dips lead to the counterstreamings and the illusion of rotation. It is noted that the oscillation period is typical for filament longitudinal oscillations, where gravity serves as the restoring force (Luna & Karpen 2012; Zhang et al. 2012).

While the longitudinal oscillations of the threads inside the filament feet are a sound explanation for avoiding the over-accumulation of magnetic twist in the filaments, spectral observations, however, did not always show alternating blue- and red-shifts quasi-periodically. For example, Yang et al. (2018) used IRIS data to analyze the profiles of the Mg II k 2796 Å and Si IV 1393 Å lines, which correspond to the cool plasmas with temperatures of 10^4 K–10^5 K. As depicted in the left panel of Figure 7, although some small patches did feature alternating blue- and red-shifts, they found coherent and stable redshifts and blueshifts across the tornado axis for more than 2.5 h, which is several times longer than the typical period of filament barb longitudinal oscillations (Li & Zhang 2013). Therefore, they tend to favor these tornadoes as flowing cool plasmas along a relatively stable helical magnetic structure. In our view, while their persistent blue- and red-shifts across the tornado axis definitely cannot be explained by the thread longitudinal oscillation model, it might still be consistent with the counterstreaming model. As we discussed in Section 3.5, there are two types of counterstreamings, i.e., longitudinal oscillations of the cold threads out of phase and spatially alternating unidirectional flows. The latter, which is due to siphon flows or jets, can last for a long time, as proposed by Chen et al. (2014) and observationally confirmed by Li & Zhang (2016). Similar persistent forward and backward flows on the two edges of a filament were confirmed in 3D MHD simulations (Xia & Keppens 2016a; Xia et al. 2017) and observations (Zou et al. 2017). The formation of a tornado associated with coronal sub-jets found by Chen et al. (2017a) might also be indirect evidence of the spatially alternating unidirectional flows as one formation mechanism of solar tornados. Moreover, the right panel of Figure 7 displays a spiral pattern in the Dopplergram revealed by Bak-Stęślicka et al. (2013) and Chen et al. (2018b). We tend to attribute it to spatially alternating unidirectional flows along a flux rope.

How solar tornados disappear is another topic worth investigating. Li & Zhang (2013) concluded that the disappearance of filament feet (here we presume that all filament feet are tornados, though rotating motions are not clearly visible in some feet possibly due to their small sizes) is generally accompanied by the disappearance of the parasitic magnetic polarity nearby. This is understandable since the small magnetic dips supporting the foot threads vanish in the magnetic rearrangement following the disappearance of the parasitic polarity. Alternatively, Chen et al. (2017a) proposed that the disappearance of tornados is due to self-reconnection of the tangled magnetic fields, which were twisted by the photospheric vortex.

It is noted in passing that the solar tornados discussed above are quasi-static structures in dormant filaments. Once a filament erupts, continuing magnetic reconnection would increase the magnetic twist of the supporting magnetic flux rope, no matter whether it pre-exists or is formed during reconnection (Ouyang et al. 2015). During the eruption, some filament materials move up and some drain down along the twisted flux rope, manifesting as erupting tornados, which have been revealed by both observations (Wang et al. 2017) and MHD numerical simulations (Jiang et al. 2018).

3.7 Is Magnetic Field Deformable due to Filament Gravity

Although it has been shown that some filaments, especially quiescent prominences, are subject to Kelvin-Helmholtz instability (Li et al. 2018a) or Rayleigh-Taylor instability (Keppens & Xia 2014; Hillier 2018), where the magnetic field deforms due to plasma motion or gravity, it was not rare to be claimed in the literature that the filament gravity cannot deform magnetic field lines when the plasma β

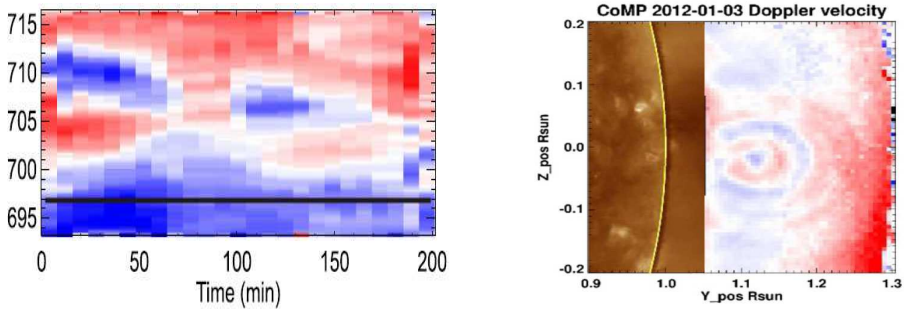

Fig. 7 *Left panel*: Time-distance diagram of the Doppler velocity along a slice across a tornado studied by Yang et al. (2018). *Right panel*: A composite image of an SDO/AIA 193 Å map (*left portion*) and the Dopplergram of a coronal cavity (*right portion*) taken and adapted from Bak-Stęślicka et al. (2013).

in the filaments is small, say 0.01–0.1. Zhou et al. (2018) pointed out that this is a misunderstanding, since the plasma β represents the strength of gas pressure compared to magnetic pressure, and has nothing to do with gravity. In order to characterize gravity, they proposed another dimensionless parameter, plasma δ, which is the ratio of gravity to magnetic pressure, i.e., $\delta = \frac{\rho g L}{B^2/2\mu_0} = 11.5 \frac{n}{10^{11}\,\mathrm{cm}^{-3}} \frac{L}{100\,\mathrm{Mm}} (\frac{B}{10\,\mathrm{G}})^{-2}$, where n is the number density of hydrogen in the prominence, L is the length of the prominence thread and B is the magnetic field. If δ is much smaller than unity, the magnetic field is not deformable because of the filament gravity. However, if δ is comparable to or larger than unity, the field lines can be deformed by the weight of filaments.

In the 2D MHD simulations of filament oscillations performed by Zhang et al. (2019), the plasma δ is $\sim$0.8. It was revealed that the magnetic field geometry changes with time as the filament oscillates along the field line (see also Kraśkiewicz et al. 2016). It is such a deformation that generates transverse oscillations of the ambient magnetic field, leading to wave leakage. The deformation of magnetic field due to filament gravity was also verified by observations, as indicated by Figure 5 in Li et al. (2018b).

4 PROSPECTS OF OTHER TOPICS

Solar filaments/prominences, objects also chased by amateurs, are full of mysteries. With large-aperture ground-based telescopes being developed and new wavelengths, in particular Lyα, being utilized in space missions like Solar Orbiter, ASOS and CHASE (Fang et al. 2019; Gan et al. 2019; Li et al. 2019a,c; Vial 2019; Vourlidas 2019), the research on solar filaments is expected to boom in the coming decade. The research on filament eruptions in other stars via LAMOST-Kepler project is also encouraged (Wang & Ip 2020). Some topics worth further exploring are summarized as follows:

– Thermal structure: Spectroscopic observations will be promising in diagnosing the thermal structure of filaments, including the distributions of temperature, density and velocity, as well as the filling factor of the threads (Heinzel et al. 2015; Ruan et al. 2019).
– Magnetic structure of the filament endpoints: In the literature it is widely believed that the magnetic field at the filament endpoints is rooted locally, meaning that the footpoints of a filament and the magnetic field line are co-spatial on the same magnetic polarity. However, for those filaments supported by flux ropes, we tend to think that the local magnetic field is a bald patch, hence the magnetic field is mainly horizontal and the real footpoint of the magnetic field line is rooted at the opposite polarity. As argued by Hao et al. (2016), considering the filament endpoints as the root of field lines would lead to mis-identification of the filament chirality. Note here that the statement does not hold true for jet-like filaments (Wang 1999).
– Filament interactions: There are many sympathetic eruptions, where eruption of one filament triggers the other (Jiang et al. 2011; Yang et al. 2012; Li et al. 2017; Hou et al. 2020). There are more events where two filaments interact rather gently, leading to rich phenomena (Jiang et al. 2013; Kong et al. 2013; Dai et al. 2018; Song et al. 2019b), which can be explored further.
– *p*-mode waves: The photospheric *p*-mode waves can easily leak to the filaments since the field lines are strongly oblique. A relationship should exist between *p*-mode waves and the filament formation and dynamics (Cao et al. 2010; Li & Zhang 2016). More simulations are encouraged.
– 3D construction of the height and shape: Rotation of activated filaments can tell the sign of helicity of the embedded magnetic field. However, 2D images might cheat our eyes as demonstrated by a famous animation picture, where a feature resembling a dancing girl can be recognized to rotate clockwise or counterclockwise. In this sense, 3D construction of the filament shapes and motions based on stereoscopic or spectroscopic observations is important (Li et al. 2010b, 2011; Song et al. 2018; Zhou et al. 2020b).

– Allowance height: Observations indicated that most prominences have an upper edge below 50 Mm, and the maximum height of the upper edge of quiescent prominences is ∼500 Mm (Wang et al. 2010). For the injection mechanism, Zou et al. (2019a) estimated that the maximum height is about 25 Mm. One question can be readily asked: what is the maximum height in the solar corona for a prominence to form via the evaporation–condensation mechanism? We are reminded that a prominence might be lifted to a higher altitude after birth due to quasi-static evolution of the magnetic field. Another question is at which height a prominence would become unstable (Liu et al. 2012a).
– Mini-filaments: It seems that mini-filaments resemble large filaments in many ways, including their eruptions as mini-CMEs (Hong et al. 2011; Yang et al. 2015a; Hong et al. 2016) and mini-ICMEs (Wang et al. 2019a). Future large telescopes can reveal more details in mini-filaments.
– Automated data processing: Over a century-long data archive of filament observations has been set up, where Hα data from worldwide observatories were collected (Lin et al. 2020). Owing to the huge amount of data, automated recognition or machine-learning methods were developed and should be improved further (Hao et al. 2013; Zhu et al. 2019), in order to statistically study the length, location, orientation and latitude migration (Gao et al. 2012).

Acknowledgements Our research was supported by the National Natural Science Foundation of China (NSFC 11533005, 11961131002, 11733003 and U1731241). X.A.A. was supported by the Science and Technology Development Fund of Macau (275/2017/A). PFC thanks ISSI-Beijing and ISSI for supporting team meetings on solar filaments. This paper is dedicated to Prof. Yunchun Jiang, who trained many students in the filament research.

References

Adrover-González, A., & Terradas, J. 2020, A&A, 633, A113
Antiochos, S. K. 2013, ApJ, 772, 72
Antiochos, S. K., MacNeice, P. J., & Spicer, D. S. 2000, ApJ, 536, 494
Arregui, I., Oliver, R., & Ballester, J. L. 2018, Living Reviews in Solar Physics, 15, 3
Aulanier, G., & Demoulin, P. 1998, A&A, 329, 1125
Awasthi, A. K., Liu, R., & Wang, Y. 2019, ApJ, 872, 109
Bak-Stęślicka, U., Gibson, S. E., Fan, Y., et al. 2013, ApJL, 770, L28
Berger, T. E., Liu, W., & Low, B. C. 2012, ApJL, 758, L37
Berger, T., Testa, P., Hillier, A., et al. 2011, Nature, 472, 197
Bi, Y., Jiang, Y., Li, H., Hong, J., & Zheng, R. 2012, ApJ, 758, 42
Bi, Y., Jiang, Y., Yang, J., et al. 2014, ApJ, 790, 100
Bi, Y., Jiang, Y., Yang, J., et al. 2015, ApJ, 805, 48
Bi, Y., Jiang, Y., Yang, J., et al. 2013, ApJ, 773, 162
Cao, W., Ning, Z., Goode, P. R., Yurchyshyn, V., & Ji, H. 2010, ApJL, 719, L95
Chae, J., Moon, Y.-J., & Park, Y.-D. 2005, ApJ, 626, 574
Chen, H., Duan, Y., Yang, J., Yang, B., & Dai, J. 2018a, ApJ, 869, 78
Chen, H., Ma, S., & Zhang, J. 2013, ApJ, 778, 70
Chen, H., Zhang, J., Ma, S., Yan, X., & Xue, J. 2017a, ApJL, 841, L13
Chen, H., Zheng, R., Li, L., et al. 2019, ApJ, 871, 229
Chen, J., Xie, W., Zhou, Y., et al. 2017b, Ap&SS, 362, 165
Chen, P. F. 2011, Living Reviews in Solar Physics, 8
Chen, P. F. 2019, Chinese Science Bulletin, 64, 3830
Chen, P. F., Harra, L. K., & Fang, C. 2014, ApJ, 784, 50
Chen, P. F., Innes, D. E., & Solanki, S. K. 2008, A&A, 484, 487
Chen, Y., Tian, H., Su, Y., et al. 2018b, ApJ, 856, 21
Cheng, X., Ding, M. D., Zhang, J., et al. 2014a, ApJL, 789, L35
Cheng, X., Ding, M. D., Zhang, J., et al. 2014b, ApJ, 789, 93
Cheng, X., Guo, Y., & Ding, M. 2017, Science China Earth Sciences, 60, 1383
Claes, N., Keppens, R., & Xia, C. 2020, A&A, 636, A112
Dai, J., Yang, J., Li, L., & Zhang, J. 2018, ApJ, 869, 118
de Jager, C. 1959, Handbuch der Physik, 52, 80
Diercke, A., Kuckein, C., Verma, M., & Denker, C. 2018, A&A, 611, A64
Duan, A., Jiang, C., He, W., et al. 2019, ApJ, 884, 73
Fan, Y. 2020, ApJ, 898, 34
Fang, C., Gu, B., Yuan, X., et al. 2019, Scientia Sinica Physica, Mechanica & Astronomica, 49, 059603
Filippov, B. 2020, MNRAS, 494, 2166
Gan, W.-Q., Zhu, C., Deng, Y.-Y., et al. 2019, RAA (Research in Astronomy and Astrophysics), 19, 156
Gao, P. X., Shi, X. J., & Li, Y. 2012, Astronomische Nachrichten, 333, 576
Gibson, S. E. 2018, Living Reviews in Solar Physics, 15, 7
Guo, Y., Cheng, X., & Ding, M. 2017, Science China Earth Sciences, 60, 1408
Guo, Y., Schmieder, B., Démoulin, P., et al. 2010, ApJ, 714, 343
Guo, Y., Xu, Y., Ding, M. D., et al. 2019, ApJL, 884, L1
Hanaoka, Y., & Sakurai, T. 2017, ApJ, 851, 130
Hao, Q., Fang, C., Cao, W., & Chen, P. F. 2015, ApJS, 221, 33
Hao, Q., Fang, C., & Chen, P. F. 2013, Sol. Phys., 286, 385
Hao, Q., Guo, Y., Fang, C., Chen, P.-F., & Cao, W.-D. 2016, RAA (Research in Astronomy and Astrophysics), 16, 1
Heinzel, P., Anzer, U., & Schmieder, B. 2003, Sol. Phys., 216, 159
Heinzel, P., Schmieder, B., Mein, N., & Gunár, S. 2015, ApJL, 800, L13
Hillier, A. 2018, Reviews of Modern Plasma Physics, 2, 1
Hong, J., Jiang, Y., Yang, J., et al. 2016, ApJ, 830, 60
Hong, J., Jiang, Y., Zheng, R., et al. 2011, ApJL, 738, L20
Hood, A. W., & Priest, E. R. 1981, Geophysical and Astrophysical Fluid Dynamics, 17, 297
Hou, Y. J., Li, T., Song, Z. P., & Zhang, J. 2020, A&A, 640, A101
Hou, Y. J., Li, T., & Zhang, J. 2016, A&A, 592, A138

Jiang, C., Feng, X., & Hu, Q. 2018, ApJ, 866, 96
Jiang, C., Wu, S. T., Feng, X., & Hu, Q. 2014a, ApJL, 786, L16
Jiang, Y., Hong, J., Yang, J., et al. 2013, ApJ, 764, 68
Jiang, Y., Yang, J., Hong, J., Bi, Y., & Zheng, R. 2011, ApJ, 738, 179
Jiang, Y., Yang, J., Wang, H., et al. 2014b, ApJ, 793, 14
Jing, J., Li, Q., Liu, C., et al. 2019, ApJ, 880, 143
Kaneko, T., & Yokoyama, T. 2017, ApJ, 845, 12
Karpen, J. T., Antiochos, S. K., Hohensee, M., Klimchuk, J. A., & MacNeice, P. J. 2001, ApJL, 553, L85
Keppens, R., & Xia, C. 2014, ApJ, 789, 22
Kliem, B., Török, T., Titov, V. S., et al. 2014, ApJ, 792, 107
Klimchuk, J. A. 2019, Sol. Phys., 294, 173
Knizhnik, K. J., Antiochos, S. K., & DeVore, C. R. 2017, ApJ, 835, 85
Kong, D.-F., Qu, Z.-N., & Guo, Q.-L. 2015, RAA (Research in Astronomy and Astrophysics), 15, 77
Kong, D. F., Yan, X. L., & Xue, Z. K. 2013, Ap&SS, 348, 303
Kraśkiewicz, J., Murawski, K., Solov'ev, A., & Srivastava, A. K. 2016, Sol. Phys., 291, 429
Kucera, T. A., Ofman, L., & Tarbell, T. D. 2018, ApJ, 859, 121
Lee, L. C., Choe, G. S., & Akasofu, S. I. 1995, Washington DC American Geophysical Union Geophysical Monograph Series, 86, 29
Li, C., Fang, C., Li, Z., et al. 2019a, RAA (Research in Astronomy and Astrophysics), 19, 165
Li, D., Shen, Y., Ning, Z., Zhang, Q., & Zhou, T. 2018a, ApJ, 863, 192
Li, H., Liu, Y., Tam, K. V., Zhao, M., & Zhang, X. 2018b, Ap&SS, 363, 118
Li, H., Yang, J., Hong, J., & Chen, H. 2019b, ApJL, 886, L34
Li, H., Chen, B., Feng, L., et al. 2019c, RAA (Research in Astronomy and Astrophysics), 19, 158
Li, K. J., Liu, X. H., Gao, P. X., & Zhan, L. S. 2010a, New Astron., 15, 346
Li, L., Peter, H., Chitta, L. P., et al. 2019d, ApJ, 884, 34
Li, L., & Zhang, J. 2013, Sol. Phys., 282, 147
Li, L., Zhang, J., Peter, H., et al. 2016, Nature Physics, 12, 847
Li, S., Su, Y., Zhou, T., et al. 2017, ApJ, 844, 70
Li, T., & Zhang, J. 2012, ApJL, 760, L10
Li, T., & Zhang, J. 2016, A&A, 589, A114
Li, T., Zhang, J., Zhang, Y., & Yang, S. 2011, ApJ, 739, 43
Li, T., Zhang, J., Zhao, H., & Yang, S. 2010b, ApJ, 720, 144
Li, X., Morgan, H., Leonard, D., & Jeska, L. 2012, ApJL, 752, L22
Liakh, V., Luna, M., & Khomenko, E. 2020, A&A, 637, A75
Lin, G., Zhu, G., Yang, X., et al. 2020, ApJS, 249, 11
Lin, Y., Engvold, O., Rouppe van der Voort, L., Wiik, J. E., & Berger, T. E. 2005, Sol. Phys., 226, 239
Liu, K., Wang, Y., Shen, C., & Wang, S. 2012a, ApJ, 744, 168
Liu, R. 2020, RAA (Research in Astronomy and Astrophysics), 20, 165
Liu, R., Chen, J., & Wang, Y. 2018a, Science China Physics, Mechanics, and Astronomy, 61, 69611
Liu, R., Liu, C., Xu, Y., et al. 2013, ApJ, 773, 166
Liu, T., Su, Y., Cheng, X., van Ballegooijen, A., & Ji, H. 2018b, ApJ, 868, 59
Liu, W., Berger, T. E., & Low, B. C. 2012b, ApJL, 745, L21
Liu, Z., Xu, J., Gu, B.-Z., et al. 2014, RAA (Research in Astronomy and Astrophysics), 14, 705
Low, B. C. 2015, Science China Physics, Mechanics, and Astronomy, 58, 5626
Luna, M., & Karpen, J. 2012, ApJL, 750, L1
Mackay, D. H., Schmieder, B., López Ariste, A., & Su, Y. 2020, A&A, 637, A3
Malherbe, J. M. 1989, Astrophysics and Space Science Library, 150, The Formation of Solar Prominences, ed. E. R. Priest, Dynamics and Structure of Quiescent Solar Prominences, 115
Martin, S. F. 1998, in Astronomical Society of the Pacific Conference Series, 150, IAU Colloq. 167: New Perspectives on Solar Prominences, eds. D. F. Webb, B. Schmieder, & D. M. Rust, 419
Martin, S. F., Marquette, W. H., & Bilimoria, R. 1992, in Astronomical Society of the Pacific Conference Series, 27, The Solar Cycle, ed. K. L. Harvey, 53
Mazumder, R., Pant, V., Luna, M., & Banerjee, D. 2020, A&A, 633, A12
Mei, Z. X., Keppens, R., Roussev, I. I., & Lin, J. 2017, A&A, 604, L7
Mei, Z. X., Keppens, R., Roussev, I. I., & Lin, J. 2018, A&A, 609, A2
Ouyang, Y., Chen, P. F., Fan, S. Q., Li, B., & Xu, A. A. 2020, ApJ, 894, 64
Ouyang, Y., Yang, K., & Chen, P. F. 2015, ApJ, 815, 72
Ouyang, Y., Zhou, Y. H., Chen, P. F., & Fang, C. 2017, ApJ, 835, 94
Panasenco, O., Martin, S. F., & Velli, M. 2014, Sol. Phys., 289, 603
Panesar, N. K., Tiwari, S. K., Moore, R. L., & Sterling, A. C. 2020, ApJL, 897, L2
Pant, V., Mazumder, R., Yuan, D., et al. 2016, Sol. Phys., 291, 3303
Pant, V., Srivastava, A. K., Banerjee, D., et al. 2015, RAA (Research in Astronomy and Astrophysics), 15, 1713
Parenti, S. 2014, Living Reviews in Solar Physics, 11, 1
Parker, E. N. 1953, ApJ, 117, 431
Pettit, E. 1932, ApJ, 76, 9
Pike, C. D., & Mason, H. E. 1998, Sol. Phys., 182, 333
Ruan, G., Jejčič, S., Schmieder, B., et al. 2019, ApJ, 886, 134
Ruan, G., Schmieder, B., Mein, P., et al. 2018, ApJ, 865, 123
Ruderman, M. S., & Luna, M. 2016, A&A, 591, A131
Rust, D. M., & Kumar, A. 1994, Sol. Phys., 155, 69
Schmieder, B., Aulanier, G., & Vršnak, B. 2015, Sol. Phys., 290, 3457
Schmieder, B., Mein, P., Mein, N., et al. 2017, A&A, 597, A109
Schmieder, B., Raadu, M. A., & Wiik, J. E. 1991, A&A, 252, 353
Schmieder, B., Tian, H., Kucera, T., et al. 2014, A&A, 569, A85
Shen, Y., Ichimoto, K., Ishii, T. T., et al. 2014a, ApJ, 786, 151
Shen, Y., Liu, Y. D., Chen, P. F., & Ichimoto, K. 2014b, ApJ, 795, 130

Shen, Y., Liu, Y., Liu, Y. D., et al. 2015, ApJL, 814, L17
Shen, Y., Qu, Z., Yuan, D., et al. 2019, ApJ, 883, 104
Song, H. Q., Chen, Y., Zhang, J., et al. 2015, ApJL, 804, L38
Song, H. Q., Zhang, J., Cheng, X., et al. 2019a, ApJ, 883, 43
Song, H. Q., Chen, Y., Li, B., et al. 2017, ApJL, 836, L11
Song, H. Q., Zhou, Z. J., Li, L. P., et al. 2018, ApJL, 864, L37
Song, Z., Hou, Y., & Zhang, J. 2019b, ApJ, 871, 7
Spicer, D. S., Feldman, U., Widing, K. G., & Rilee, M. 1998, ApJ, 494, 450
Su, Y., Gömöry, P., Veronig, A., et al. 2014, ApJL, 785, L2
Su, Y., Liu, R., Li, S., et al. 2018, ApJ, 855, 77
Su, Y., van Ballegooijen, A., McCauley, P., et al. 2015, ApJ, 807, 144
Su, Y., Wang, T., Veronig, A., Temmer, M., & Gan, W. 2012, ApJL, 756, L41
Tandberg-Hanssen, E. 1974, Solar Prominences, 12
Vial, J.-C. 2019, RAA (Research in Astronomy and Astrophysics), 19, 166
Vial, J.-C., & Engvold, O. 2015, Solar Prominences, 415
Vourlidas, A. 2019, RAA (Research in Astronomy and Astrophysics), 19, 168
Wang, B., Chen, Y., Fu, J., et al. 2016a, ApJL, 827, L33
Wang, H., Liu, R., Li, Q., et al. 2018a, ApJL, 852, L18
Wang, J. M., Feng, H. Q., Li, H. B., et al. 2019a, ApJ, 876, 57
Wang, J. X., & Ip, W.-H. 2020, RAA (Research in Astronomy and Astrophysics), 20, 157
Wang, J., Yan, X., Guo, Q., et al. 2019b, MNRAS, 488, 3794
Wang, J., Yan, X., Qu, Z., et al. 2018b, ApJ, 863, 180
Wang, W., Liu, R., & Wang, Y. 2017, ApJ, 834, 38
Wang, Y.-M. 1999, ApJL, 520, L71
Wang, Y. M., Muglach, K., & Kliem, B. 2009, ApJ, 699, 133
Wang, Y., Cao, H., Chen, J., et al. 2010, ApJ, 717, 973
Wang, Y., Zhang, Q., Liu, J., et al. 2016b, Journal of Geophysical Research (Space Physics), 121, 7423
Wei, H., Huang, Z., Hou, Z., et al. 2020, MNRAS, 498, L104
Wittmann, A. D., & Xu, Z. T. 1987, A&AS, 70, 83
Xia, C., Chen, P. F., Keppens, R., & van Marle, A. J. 2011, ApJ, 737, 27
Xia, C., & Keppens, R. 2016a, ApJ, 823, 22
Xia, C., & Keppens, R. 2016b, ApJL, 825, L29
Xia, C., Keppens, R., Antolin, P., & Porth, O. 2014, ApJL, 792, L38
Xia, C., Keppens, R., & Fang, X. 2017, A&A, 603, A42
Xing, C., Li, H. C., Jiang, B., Cheng, X., & Ding, M. D. 2018, ApJL, 857, L14
Xu, H., Su, J., Chen, J., et al. 2020, arXiv e-prints, arXiv:2008.08299
Xu, Z., Lagg, A., Solanki, S., & Liu, Y. 2012, ApJ, 749, 138
Xue, Z., Yan, X., Cheng, X., et al. 2016, Nature Communications, 7, 11837
Yan, X. L., Priest, E. R., Guo, Q. L., et al. 2016, ApJ, 832, 23
Yan, X. L., Xue, Z. K., Liu, J. H., Kong, D. F., & Xu, C. L. 2014, ApJ, 797, 52
Yan, X.-L., Xue, Z.-K., Xiang, Y.-Y., & Yang, L.-H. 2015, RAA (Research in Astronomy and Astrophysics), 15, 1725
Yan, X., Xue, Z., Cheng, X., et al. 2020, ApJ, 889, 106
Yang, B., Jiang, Y., Yang, J., Bi, Y., & Li, H. 2016a, ApJ, 830, 16
Yang, B., Jiang, Y., Yang, J., Hong, J., & Xu, Z. 2015a, ApJ, 803, 86
Yang, B., Jiang, Y., Yang, J., Yu, S., & Xu, Z. 2016b, ApJ, 816, 41
Yang, J., Jiang, Y., Xu, Z., Bi, Y., & Hong, J. 2015b, ApJ, 803, 68
Yang, J., Jiang, Y., Zheng, R., et al. 2012, ApJ, 745, 9
Yang, S., Zhang, J., Liu, Z., & Xiang, Y. 2014, ApJL, 784, L36
Yang, Z., Tian, H., Peter, H., et al. 2018, ApJ, 852, 79
Zhang, L. Y., Fang, C., & Chen, P. F. 2019, ApJ, 884, 74
Zhang, Q. M., Chen, P. F., Guo, Y., Fang, C., & Ding, M. D. 2012, ApJ, 746, 19
Zhang, Q. M., Chen, P. F., Xia, C., Keppens, R., & Ji, H. S. 2013, A&A, 554, A124
Zhang, Q. M., Guo, J. H., Tam, K. V., & Xu, A. A. 2020a, A&A, 635, A132
Zhang, Q. M., & Ji, H. S. 2018, ApJ, 860, 113
Zhang, Q. M., Li, D., & Ning, Z. J. 2017a, ApJ, 851, 47
Zhang, Q. M., Li, T., Zheng, R. S., Su, Y. N., & Ji, H. S. 2017b, ApJ, 842, 27
Zhang, Q. M., Ning, Z. J., Guo, Y., et al. 2015, ApJ, 805, 4
Zhang, Q., Wang, Y., Liu, R., et al. 2020b, ApJL, 898, L12
Zhao, X., Xia, C., Keppens, R., & Gan, W. 2017, ApJ, 841, 106
Zheng, R., Zhang, Q., Chen, Y., et al. 2017, ApJ, 836, 160
Zheng, R., Yang, S., Rao, C., et al. 2019, ApJ, 875, 71
Zhou, Y. H., Chen, P. F., Hong, J., & Fang, C. 2020a, Nature Astronomy
Zhou, Y.-H., Chen, P.-F., Zhang, Q.-M., & Fang, C. 2014, RAA (Research in Astronomy and Astrophysics), 14, 581
Zhou, Y.-H., Xia, C., Keppens, R., Fang, C., & Chen, P. F. 2018, ApJ, 856, 179
Zhou, Y.-H., Zhang, L.-Y., Ouyang, Y., Chen, P. F., & Fang, C. 2017, ApJ, 839, 9
Zhou, Z., Cheng, X., Zhang, J., et al. 2019, ApJL, 877, L28
Zhou, Z., Liu, R., Cheng, X., et al. 2020b, ApJ, 891, 180
Zhu, C., Liu, R., Alexander, D., Sun, X., & McAteer, R. T. J. 2015, ApJ, 813, 60
Zhu, G., Lin, G., Wang, D., Liu, S., & Yang, X. 2019, Sol. Phys., 294, 117
Zhu, X., Wiegelmann, T., & Solanki, S. K. 2020, A&A, 640, A103
Zirin, H. 1988, Astrophysics of the sun
Zirker, J. B., Engvold, O., & Martin, S. F. 1998, Nature, 396, 440
Zou, P., Fang, C., Chen, P. F., Yang, K., & Cao, W. 2017, ApJ, 836, 122
Zou, P., Fang, C., Chen, P. F., et al. 2016, ApJ, 831, 123
Zou, P., Jiang, C.-W., Wei, F.-S., & Cao, W.-D. 2019a, RAA (Research in Astronomy and Astrophysics), 19, 084
Zou, P., Jiang, C., Wei, F., Zuo, P., & Wang, Y. 2019b, ApJ, 884, 157